1-1-2010

Synthesis and electrochemical studies on Li2CuSnO4 and Li2CuSnSiO6 as negative electrode in lithium batteries

Atef Y. Shenouda
Central Metallurgical Research and Development Institute

Hua-Kun Liu
University of Wollongong, hua@uow.edu.au

Synthesis and electrochemical studies on Li2CuSnO4 and Li2CuSnSiO6 as negative electrode in lithium batteries

Abstract

Li_2CuSnO_4 and $Li_2CuSnSiO_6$ were prepared from their precursors compounds using Brij surfactant and a hydrothermal autoclave method. X-ray diffraction characterization revealed that the crystal structures of these compounds were tetragonal. Scanning electron microscope investigation showed the particle size morphology of $Li_2CuSnSiO_6$ is larger than that of Li_2CuSnO_4. Electrochemical impedance spectroscopy (EIS) explained that Li_2CuSnO_4 cell had higher charge transfer resistance (R_{ct} = 2936Ω) than that of $Li_2CuSnSiO_6$ (38Ω). Furthermore, the reversible specific discharge capacity of the $Li_2CuSnSiO_6$ cell was 870 mAh/g in comparison with 780 mAh/g for the Li_2CuSnO_4 cell after 100 cycles.

Keywords

Synthesis, electrochemical, studies, Li2CuSnO4, Li2CuSnSiO6, negative, electrode, lithium, batteries

Disciplines

Engineering | Physical Sciences and Mathematics

Publication Details

Shenouda, AY & Liu, HK (2010), Synthesis and electrochemical studies on Li_2CuSnO_4 and $Li_2CuSnSiO_6$ as negative electrode in lithium batteries, Rechargeable Lithium and Lithium-Ion Batteries - 216th ECS Meeting, pp. 75-89, Pennington, NJ, USA: The Electrochemical Society.

ECS Transactions, 25 (36) 75-89 (2010)
10.1149/1.3393842 ©The Electrochemical Society

Synthesis and Electrochemical Studies on Li_2CuSnO_4 and $Li_2CuSnSiO_6$ as negative electrode in the lithium batteries

Atef Y. Shenouda [a, *] and Hua Kun Liu [b]

a Central Metallurgical Research and Development Institute (CMRDI), Tebbin, P.O. Box 87 Helwan, Egypt.

b Institute for Superconducting and Electronic Materials, ARC Centre of Excellence for Electro materials Science, University of Wollongong, NSW 2522, Australia

Abstract

Li_2CuSnO_4 and $Li_2CuSnSiO_6$ were prepared from their precursors compounds using Brij surfactant and a hydrothermal autoclave method. . X-ray diffraction characterization revealed that the crystal structures of these compounds were tetragonal. Scanning electron microscope investigation showed the particle size morphology of $Li_2CuSnSiO_6$ is larger than that of Li_2CuSnO_4. Electrochemical impedance spectroscopy (EIS) explained that Li_2CuSnO_4 cell had higher charge transfer resistance (**R_{ct} = 2936Ω**) than that of $Li_2CuSnSiO_6$ (**38Ω**). Furthermore, the reversible specific discharge capacity of the $Li_2CuSnSiO_6$ cell was 870 mAh/g in comparison with 780 mAh/g for the Li_2CuSnO_4 cell after 100 cycles.

[*]Corresponding author:

- **Tel: 00202 25010642 /3 Fax: 00202 25010639**
- **E-mail: ayshenouda@yahoo.com**

1. Introduction

Rechargeable lithium batteries have been considered an attractive power source for a wide variety of applications in popular electronic devices such as mobile telephones, video tape recorders and laptop computers. Nowadays, these batteries are being scaled-up for prospective use in electric vehicles and energy storage. Therefore, the development of lithium batteries into advanced utilities is considered an important goal to meet a great demand. Different types of active materials have been investigated for both positive and negative electrodes [1-8].

In order to develop high capacity anode for lithium ion batteries, silicon and some metals that can alloy with lithium at a high molar ratio are being exploited and developed as promising anode materials [9].

Fine powders of tin oxide doped with traces of silicon in combination with highly dispersed amorphous silicon oxide have been synthesized by an advanced ultrasonic spray method [10]. The electrochemical results showed that addition of silicon decreases the tin oxidation state, and hence, reduces the irreversible capacity during the first discharge/charge cycle. SiO_2 and Li_2SiO_3 appeared during the first discharge, as confirmed by infrared (IR) spectroscopy. Furthermore, a reversible capacity was found of 900 mAh/g to 950 mAh/g for these composites. This improved performance was due to enhanced interfacial diffusion caused by highly dispersed inert second phases, i.e., SiO_2 and $LiSi_2O_3$. It was found that when the silicon content in the precursor was high enough, some metallic tin appeared in the product. This means that addition of some SiO_2 to the precursor will reduce the oxygen content of the final product. Since the oxygen bound to Sn is responsible for the observed irreversible capacity, a low oxidation state is highly beneficial for this anode material.

We can also see that the introduction of SiO_2 into the $Li_2O–CuO–SnO_2$ system will improve the specific capacity through the intercalation and de-intercalation of Li with Si. This study is an attempt to study the electrochemical performance of this quaternary metal oxide system ($Li_2O–CuO–SnO_2$-SiO_2). Also, the amount of reported literature on this system is small, and more data are needed.

2. Experimental

2.1. *Materials preparation*

Stoichiometric amounts of CH_3COOLi (Alfa Aesar), $(CH_3CO_2)_2Cu$ (Aldrich), and stannous oxalate (Aldrich) were dissolved separately in distilled water to prepare Li_2CuSnO_4. Brij 30 [CH_3 $(CH_2)_{10}CH_2$ $(OCH_2$ $CH_2)_4OH$] surfactant was added in a weight ratio of 5: 1 wt. / wt. with respect to the active materials. In order to prepare $Li_2CuSnSiO_6$, we used Si_3N_4 (Nanostructured and Amorphous materials Inc., USA, 15 nm). The raw material compounds were then mixed together. The mixed solution was stirred and heat-treated at 80°C for 2 hours. The mixture was then transferred to an autoclave vessel (250 cm^3) and heat-treated at 250°C for 10 hours. Finally, the samples were calcined in air atmosphere at 750°C for 12 h in an alumina crucible. The samples were left to cool down to room temperature inside the furnace. The samples were sintered again for another 12 h at the same temperature in air.

2.2. *Materials characterisations*

Powder X-ray diffraction (XRD) measurements were carried out using a Philips powder diffractometer with Cu K_α radiation. Infrared absorption spectra were recorded using a FT/IR-6300 type A Fourier transform infrared (FTIR) interferometer. Samples were ground to fine powders, mixed, and diluted with KBr. The IR region examined was 400–4000 cm^{-1}. Elemental compositions of the various tin oxide compounds were analysed by inductively coupled plasma (ICP, PerkinElmer Optima 2000 DV). Scanning electron microscopy (SEM) was conducted with a JEOL SEM Model 6460.

2.3. Electrochemical measurements

The homogeneous slurry used to form the electrodes was composed of 85 wt% active materials, 10 wt% acetylene black, and 5 wt% polyvinylidene fluoride (PVDF) binder dissolved in *N*-methyl pyrrolidone (NMP) solvent. It was then spread onto Cu foil substrates. The area of each coated electrode was 1 cm^2. The electrodes were dried in a vacuum oven under a vacuum pressure of 30 Torr at 110°C for 12 h. The electrodes were then pressed at a pressure of 2000 kg/cm^2. The active material loading was about 4 mg for each individual electrode. CR2032 coin cells were then assembled in an argon filled glove box (Mbraun, Unilab, Germany), using lithium metal foil as the counter electrode. The electrolyte was 1M $LiPF_6$ in a mixture of ethylene carbonate (EC) and dimethyl carbonate (DMC) (1:1 by volume, provided by MERCK). The cells were galvanostatically charged and discharged over a voltage range of 0.0–3 V using a current of 0.02 A for both processes. Cyclic voltammetry (CV) measurements were performed using a Multi-stat CHI660 Electrochemical Workstation at a 0.1 mVs^{-1} scanning rate, and the potential windows were 0 and 3 V versus Li/Li^+ electrode. The AC impedance measurement amplitude was 50 mV. The frequency range was 100 kHz – 10 mHz.

3. Results and Discussion:

3.1 Structural Characterization

X-ray diffraction patterns of the Li_2CuSnO_4 and $Li_2CuSnSiO_6$ samples showed suitable crystallinity, as shown in Fig. 1. Their structures were indexed to the tetragonal system using Rietveld analysis of the XRD pattern data with a standard software package. The refined unit cell parameters are $a = 4.752$ Å, $c = 3.203$ Å, and cell volume, $V = 72.3285$ $Å^3$ for Li_2CuSnO_4, *while* $a = 4.913$ Å, $c = 3.375$ Å, and cell volume, $V = 81.4643$ $Å^3$ for $Li_2CuSnSiO_6$. The crystallite sizes of Li_2SnCuO_4 and $Li_2CuSnSiO_6$ are 11.1836 and 28.2495 nm, respectively, according to the Debye-Scherrer equation [11]:

$$L = 0.9 \lambda / w \cos \theta \qquad [1]$$

where θ and *w* are the Bragg angle and the full width at half maximum, measured in radians, of each diffraction peak, respectively. Also, λ is the X-ray wavelength, and L is the effective particle or grain size. It is observed that the unit cell parameters of $Li_2SnCuSiO_6$ are greater in value than those of Li_2SnCuO_4.

Fig. 2 shows a SEM image of the samples. The powders have an average crystal size between 50 and 100 nm. In general, the particles have an interconnected network structure in the form of aggregates.

Fig. 3 displays FTIR spectra collected in the wave number range from 400 to 4000 cm^{-1}. The bands at 1200, 1080, 790, and 495cm^{-1} are attributed to different vibrational modes of Si–O–Si and O–Si–O groups; the vibration band at 625 cm^{-1} indicates an interaction between Sn, O, and Si, which is equivalent to a Sn–O–Si bond in the silicon doped tin oxide composite. These data are consistent with previous literature [12].

3.2. Electrochemical Impedance Spectra measurements

Electrochemical impedance spectroscopy (EIS) may be considered as one of the most sensitive tools for the study of differences in electrode behavior due to surface modification. The electrochemical impedance spectra of the cells, as presented in Fig. 4, show an intercept at high frequency on the real axis Z' for the resistance of the electrolyte, R_e, followed by a semicircle in the high-middle frequency region, and a straight line in the low frequency region. The numerical value of the diameter of the semicircle on the Z_{real} axis is approximately equal to the charge transfer resistance, R_{ct}, and therefore, it can be seen that there is a marked decrease in R_{ct} after addition of the silicon compound. The straight line in the low frequency region is attributed to the diffusion of the lithium ions into the bulk of the electrode material, or the so-called Warburg diffusion. The plot of the real part of the impedance, Z_{re}, versus the reciprocal root square of the lower angular frequencies is displayed in Fig. 5. The straight lines are attributed to the diffusion of the lithium ions into the bulk of the electrode material, or the so-called Warburg diffusion. It is observed that the Warburg impedance coefficient, σ_w is 652.82 $\Omega.cm^2.s^{-0.5}$ for the $Li_2SnCuSiO_6$ cell and it has a lower value than Li_2SnCuO_4: 1415.839 $\Omega.cm^2.s^{-0.5}$. The parameters of the equivalent circuit are presented in Table 1. Also, the diffusion coefficient values for the diffusion of the lithium ions into the bulk electrode materials have been calculated and recorded in Table 1[13].

The obtained diffusion coefficient ($8.31x10^{-14}$ cm^2s^{-1}) for the $Li_2SnCuSiO_6$ cell explains the higher mobility for Li^+ ion diffusion than in the other cell, which lacked Si. Furthermore, the exchange current density (i°) of the $Li_2SnCuSiO_6$ cell b is higher the other cell a. Therefore, the charge-transfer reaction of $Li_2SnCuSiO_6$ electrode is stronger than in the other electrode prepared for the Li_2SnCuO_4 cell a. It is observed that the double layer capacitance (C_{dl}) of cell b also has a higher value: 1.95 x 10^{-5} F.

Cyclic voltammetric measurements were carried out between 0 and 3 V as shown in Fig.6. The cyclic voltammograms of the investigated samples show a cathodic reduction peak in the range of 0.51-0.63 V. This peak is attributed to intercalation of lithium into tin to form Li_xSn compound ($1 \leq x \leq 4.4$) as observed in the literatures [3, 10]. As we have Li_2SnCuO_4 and $Li_2SnCuSiO_6$ as starting materials, therefore the reduced form will be Li_2SnCu and $Li_2SnCuSi$ compounds and their intercalation with Li^+ will be as follows [14, 15]:

$$Li_2SnCu + \mathbf{(2.4 - x)\ Li^+} + 4e \rightarrow Li_{4.4-x}Sn + Cu \quad [2]$$

$$Li_2SnCuSi + \mathbf{(2.4 - x)\ Li^+} + 4e \rightarrow Li_{4.4-x}Sn + Cu + Si \quad [3]$$

$$Si + x\ Li^+ + xe \rightarrow Li_xSi \quad [4]$$

Li_2SnCuO_4 shows three anodic oxidation peaks at 0.42, 0.85 and 1.7 V, respectively for the following reactions [7,14,15].

$Li_{4.4-x}Sn + Cu \rightarrow Li_2SnCu + (2.4-x)\ Li^+ + 2e$ E = 0.42 V [5]

$Li_2SnCu + 1.5\ O_2 \rightarrow Li_2SnCuO_3 + 2e$ E = 0.85 V [6]

$Li_2SnCuO_3 + 0.5\ O_2 \rightarrow Li_2SnCuO_4 + 2e$ E = 1.7 V [7]

$Li_2SnCuSiO_6$ shows three anodic oxidation peaks at 0.68, 1.05 and 1.85V for the de-intercalation of Li^+ from $Li_{4.4-x}Sn$ and the oxidation of $Li_2SnCuSi$ to $Li_2SnCuSiO_4$ and $Li_2SnCuSiO_6$, respectively. It is observed that there is a shift in the anodic peaks to more positive potentials. This can be attributed to the oxidation of Si to $Si^{(2-x)+}$ and Si^{4+} [15].

The first discharge capacity plateaus versus the working voltage between 3 and 0.0V are illustrated in Fig. 7. The profiles for the first reduction look fairly similar for the two samples. There is a plateau that falls in the range between 1.5 and 1.7 V vs. Li^+ for the reduction of Li_2SnCuO_4 to Li_2SnCuO_3 and $Li_2SnCuSiO_6$ to $Li_2SnCuSiO_4$. The region between 1 to 0.8 V is matching with the reduction of Li_2SnCuO_3 to Li_2SnCuO_2 and the similar Si compounds. The second plateau in the region of 0.4 -0.7 V for the reduction of Li_2SnCuO_2 to Li_2SnCu and the analogue compund $Li_2SnCuSi$. Below 0.4V, the intercalation of Li_2SnCu or $Li_2SnCuSi$ with Li ions takes place and $Li_{4.4-x}Sn$ is formed as mentioned before [14, 15].

The first discharge curve of cell "b" delivers the highest specific discharge capacity of about 1300 mAh g^{-1}. Similar results have been observed in the literature in spite of using different methods of preparation [7,12,16]. The cycling performance of these cells, as shown in Fig. 8, remained good for 140 cycles. The specific discharge capacity of the $Li_2SnCuSiO_6$ cell (b) is about 900 mAh g^{-1}, and it is higher than for cell (a). However, the discharge capacities have small decrease up to 140-150 cycles, and then followed by great decrease up to 200 cycles or more extra cycles. The excess capacity of Li_2CuSnO_4 and $Li_2CuSnSiO_6$ electrodes rather than Sn ones is attributed to the presence of Cu and Si. Probably, the formation of the Li_2SnCu or Li_2SnCu Si intermetallic phase relaxed the cracking process to a certain degree and improved the cycle life of the electrode. In comparison with the Sn electrodes, the lasts exhibit great capacity fading upon cycling as explained by S. Gopukumar et. al. [17].

It has been reported that transition metal oxides show reversible Li storage behaviour [18]. In those cases, a transition metal can react with Li_2O upon Li extraction, which means that the reduction reaction at potentials above 1 V vs. Li/Li^+ is reversible, which could contribute to a high reversible capacity [19].

It was reported that Li-O bonds are not stable when the charging voltage is above 1.3 V vs. Li/Li^+ [19]. Moreover, it was indicated that Li_2O formation reaction is reversible for most of the metal compounds in view of their thermodynamics. The reversibility of this reaction from LiX (*e.g.* Li_2O) and metal (*e.g.* Ni) back to metal compounds is mainly influenced by the intrinsic conductivity of the MX compound, the grain size of LiX , the metal, the separation distance between LiX and metal and the electronic contact with the conductive additive [20].

References

1. A. Y. Shenouda, *Electrochimica Acta*, **51**, 5973 (2006).

2. A. Y. Shenouda and K.R. Murali., *J. Power Sources*, **176**, 332 (2008).

3. A. Y. Shenouda and Hua K. Liu , *J. Power Sources*, **185**, 1386 (2008).

4. A. Y. Shenouda, Hua K. Liu, *J. Alloys and Compounds* **477**, 498 (2009).

5. A. Y. Shenouda and S. M. El-Sayed, *J. Alloys and Compounds* xxx, xxx (2010).

6. J. L. Shui, G. S. Jiang, S. Xie, C. H. Chen, *Electrochim. Acta*, **49**, 2209 (2004).

7. Y. Yu, C. H. Chen, J. L. Shui, S. Xie, Angew. *Chem. Int. Ed*. **44**, 7085 (2005).

8. Yan Yu, Chun-Hua Chen, Yi Shi, *Advanced Materials* **19**, 993 (2007).

9. Z. Wen, K. Wang, L. Chen, J. Xie, *Electrochem. Commun.* **8**, 1349 (2006).

10. H. Huang , E.M. Kelder, L. Chen , J. Schoonman, *J. Power Sources* **81–82**, 362 (1999).

11. C. Matei Ghimbeu, R.C. van Landschoot, J. Schoonman, M. Lumbreras, *J. European Ceramic* Soc., **27**, 207 (2007).

12.Y. Liang, J. Fan, X. Xia, Y. Luo, Z. Jia *Electrochimica Acta*, **52**, 5891 (2007).

13. A.J. Bard, L.R. Faulkner, Electrochemical Methods, 2nd ed., p.231, John Wiley & Sons, New York (2001).

14. D.G. Kim, H.Kim, H. J. Sohn, T. Kang, *J. Power Sources*, **104**, 221 (2002).

15. Q. Sun, B. Zhang, Zheng-Wen Fu, *Applied Surface Science* **254**, 3774 (2008).

16.Y.I. Kim, W.H. Lee, H.S. Moon, K.S. Ji, S.H. Seong and J.W. Park, *J. Power Sources*, **101**, 253 (2001).

17. A. Sivashanmugam, T. Prem Kumar, N.G. Renganathan, S. Gopukumar, M. Wohlfahrt-Mehrens , J. Garche, J. Power Sources **144**, 197–203 (2005).

18. P. Poizot, S. Laruelle, S. Grugeon, L. Dupont, J.-M. Tarascon, Nature, **407**, 496 (2000).

19. A.D´ebart, L. Dupont, P. Poizot, J.-B. Leriche, J. M. Tarascon, J. Electrochem. Soc. **148**, A1266 (2001).

20. X.H. Huang, J.P. Tu, B. Zhang, C.Q. Zhang, Y. Li, Y.F. Yuan, H.M. Wu, J. Power Sources **161**, 541 (2006).

Table 1. Impedance parameters of the cells samples.

Samples	R_e [Ω]	R_{ct} [Ω]	σ [Ω.cm^{2}s$^{-0.5}$]	D [cm^{2}s^{-1}]	C_d [F]	i^o [mA/cm^2]
Li_2CuSnO_4	730	2936	1415.839	1.77x10^{-14}	7.77E-07	7.00E-06
$Li_2CuSnSiO_6$	22	38	652.8277	8.31x10^{-14}	1.95E-05	6.75E-04

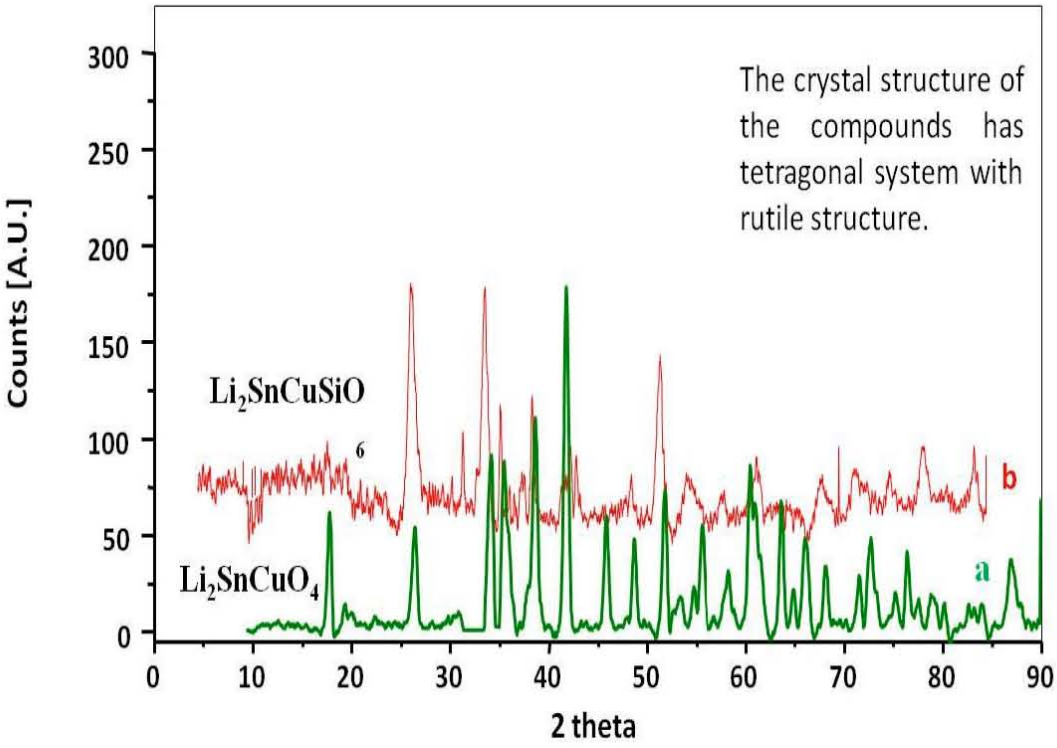

Fig. 1 XRD patterns of (a) Li_2SnCuO_4 and (b) $Li_2SiCuSnO_6$ compounds.

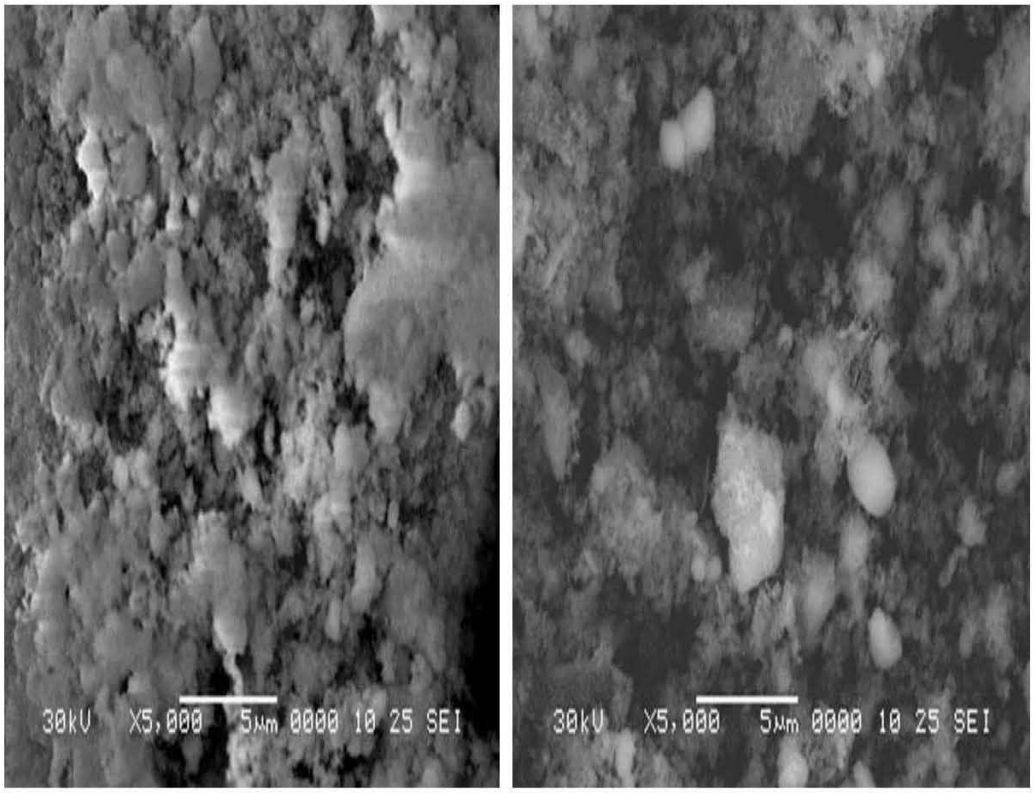

Fig.2 SEM of (a) Li_2SnCuO_4 and (b) $Li_2SiCuSnO_6$ compounds.

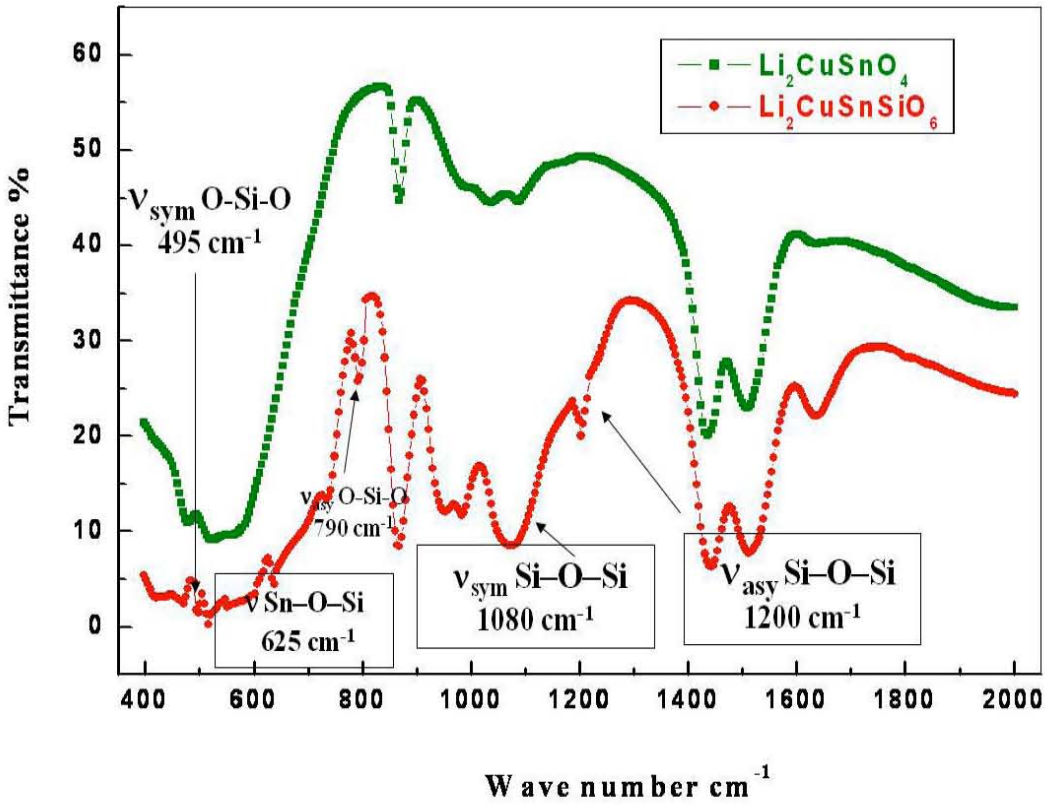

Fig. 3 FTIR spectra of the prepared (a) Li_2SnCuO_4 and (b) $Li_2SiCuSnO_6$ compounds.

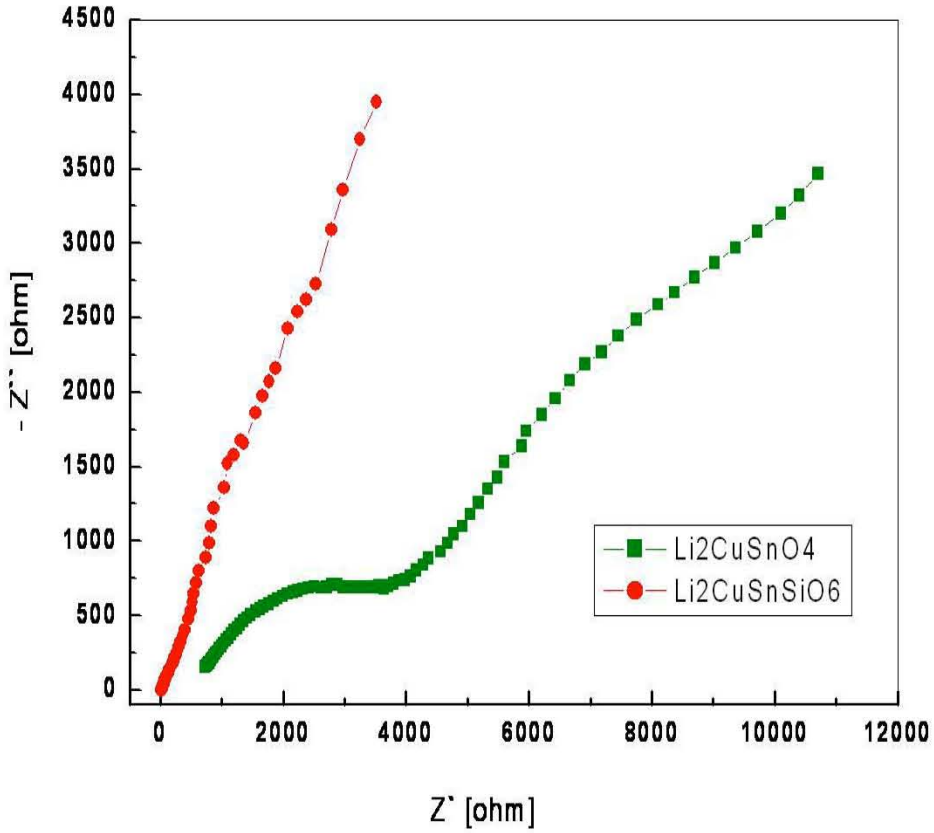

Fig. 4 EIS spectroscopy Li_2CuSnO_4 (a) and $Li_2CuSnSiO_6$ (b) Cells.

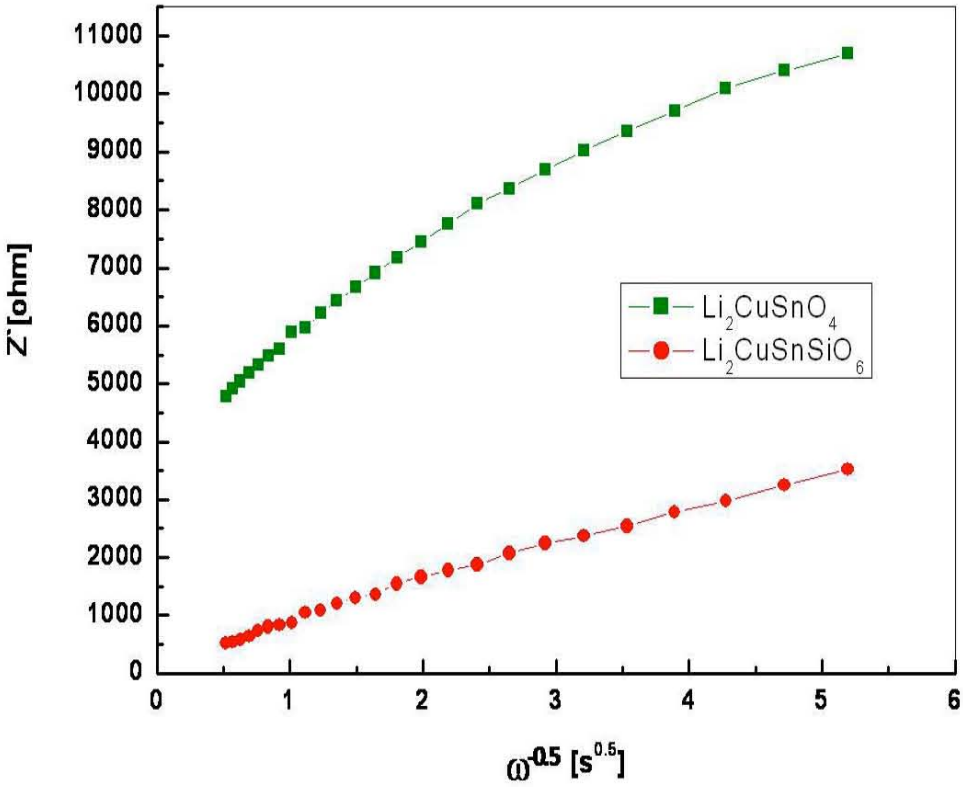

Fig. 5 Relationship between real impedance with the low frequencies for Li_2CuSnO_4 (a), $Li_2CuSnSiO_6$ (b) Cells.

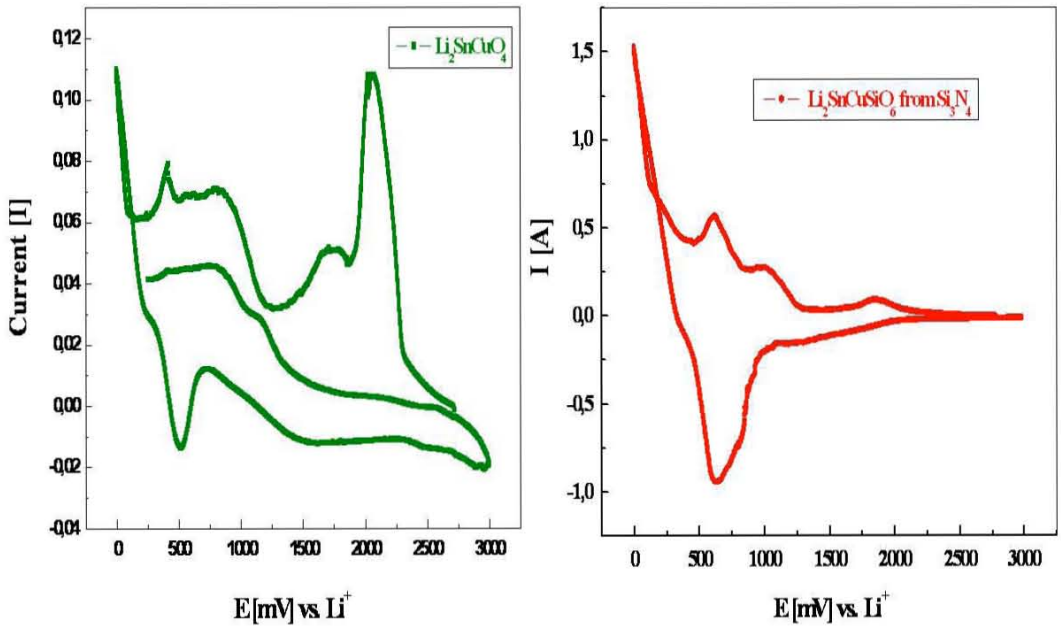

Fig. 6 Cyclic voltammograms of Li_2CuSnO_4 (a), $Li_2CuSnSiO_6$(b) cells, scan rate: 0.1 mVs^{-1}.

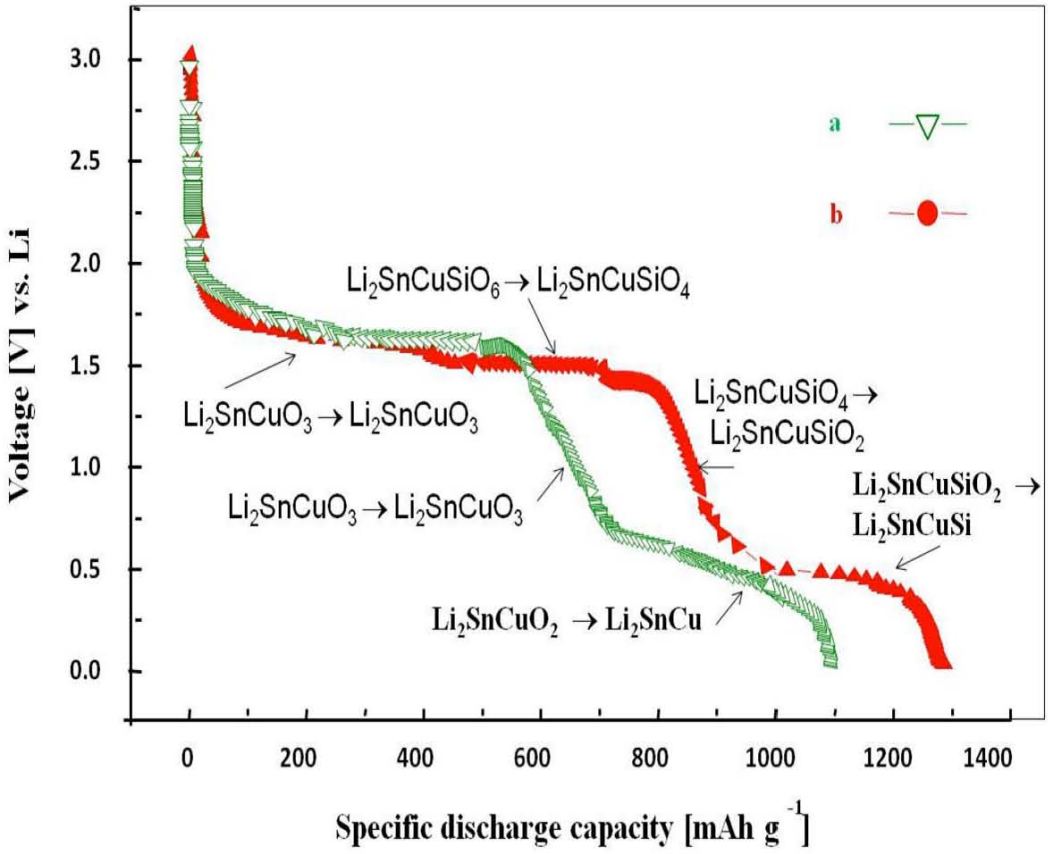

Fig. 7 First discharge voltage- capacity profile of Li_2CuSnO_4 (a) $Li_2CuSnSiO_6$ (b) cells.

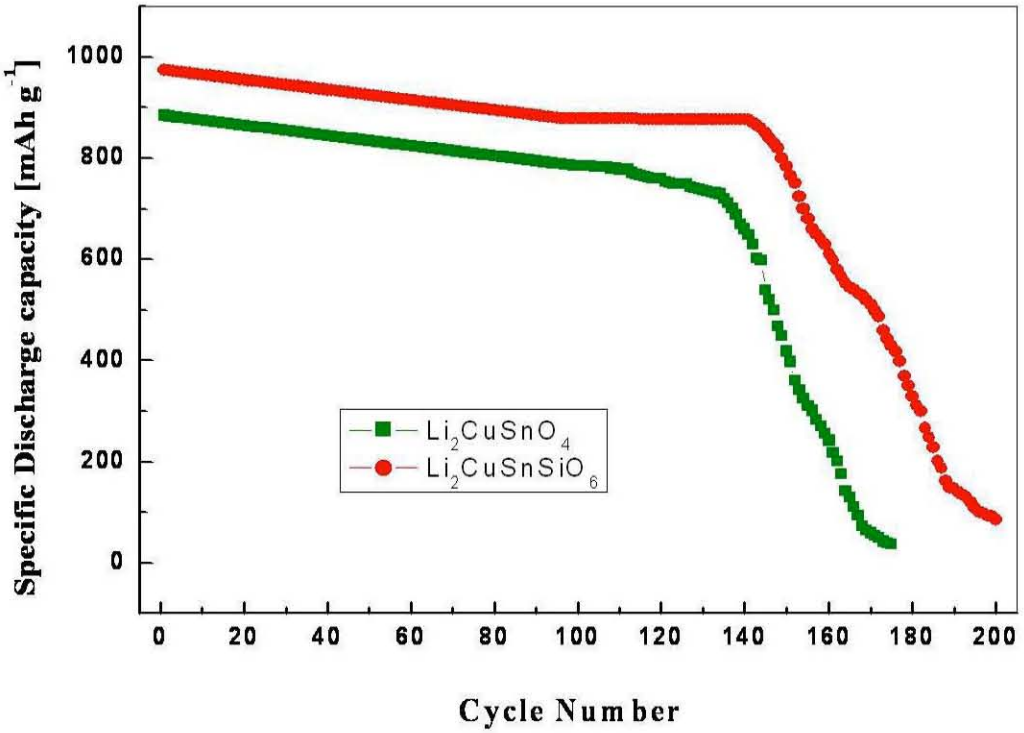

Fig. 8 Cycling performance of Li_2CuSnO_4 (a) and $Li_2CuSnSiO_6$ (b) cells.